AUTOMATIC BREAKLINE DETECTION FROM AIRBORNE LASER RANGE DATA

Regine BRÜGELMANN

Ministry of Transport, Public Works and Water Management, The Netherlands

Survey Department

Section of Remote Sensing and Photogrammetry

r.brugelmann@mdi.rws.minvenw.nl

Working Group III/5

KEY WORDS: DTM/DEM/DSM, Surface Reconstruction, Feature Extraction, Automation, Edge Extraction.

ABSTRACT

Airborne laserscanning is a relatively new and powerful technique for the acquisition of digital elevation models. Mostly they are represented by regular grids. For some purposes, however, the description of the terrain with such a regular grid is insufficient. Knowledge over the precise position of breaklines is required. Image processing algorithms can be used for automatically deriving these breaklines from laserdata In this contribution, the suitability of a method for the extraction of breaklines from dense laserdata has been investigated. It is based on hypothesis testing. All pixels with a significant homogeneity measure with respect to noise are denoted as potential edge pixels. The *quadratic variation*, used as homogeneity measure, indicates the extent of curvature. Hypothesis testing yields broad breakline-regions with significant curvature compared to noise. These regions are reduced to one pixel wide breaklines by means of nonmaxima-suppression taking into account maximal curvature direction. For the assessment of the performance of the algorithm the automatically extracted breaklines are compared with photogrammetrically measured breaklines. It is shown that automatic breakline extraction from airborne laserdata in principle is feasible.

1 INTRODUCTION

Airborne laserscanning is a relatively new and powerful technique for dense digital 3D-data acquisition. Beside applications such as derivation of building models, monitoring of power lines and extraction of forest stand attributes such as tree heights, the main application of airborne laserscanning still is the determination of digital elevation models.

Compared with traditional methods such as photogrammetry and tachimetry, laser altimetry, with its increasing operationality, has become a cost and time effective alternative for the acquisition of digital elevation models. That's why this new technique nowadays is used to build elevation models for even whole countries such as for The Netherlands. The entire surface of The Netherlands is planned to be covered with laserdata with a density of one point per 16 m^2 in 2000. From the originally irregularly distributed measured points a regular grid is derived at the Survey Department of the Ministry of Transport, Public Works and Water Management and delivered to customers such as the local water management organisations.

For some purposes, however, a regular grid on its own is insufficient for an accurate description of the terrain. This applies e.g. to road planning and road design or to computations in the field of river management, e.g. the determination of waterheights and streamvelocities in case of flooding. In these cases additional terrain shape information is required. Breaklines provide this information. Describing the upper and lower edges of geomorphological features such as dikes (see fig. 1), breaklines contain the most important morphological information of a digital elevation model. As 3D-vectors they represent local maxima of surface curvature.

Furthermore, the use of breaklines as constraints for DEM calculation considerably contributes to morphological correct DEM computation (Petzold et al., 1999). Apart from this, the automatic derivation of breakline information forms a crucial contribution to the task of data reduction. The huge amount of data acquired by laserscanners can be expected to cause difficulties in further processing, e.g. with computations concerning managing of whole rivers fluvial zones. This can be overcome by the conversion of raster or triangle representation to vector structures which forms a sort of information condensation (Weidner, 1994). The implicit, in a grid or TIN (triangulated irregular network) represented information, is transformed into explicit surface descriptions embodied by vector structures such as break-, ridge- or valleylines.

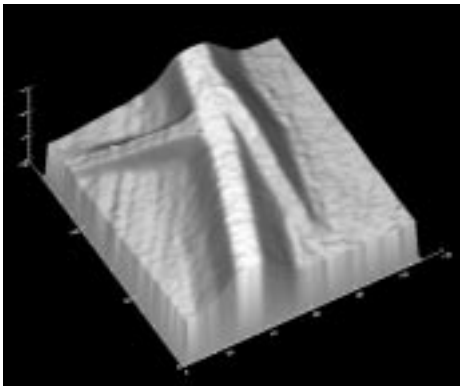

(a) Example of laserdata: dike with ascents

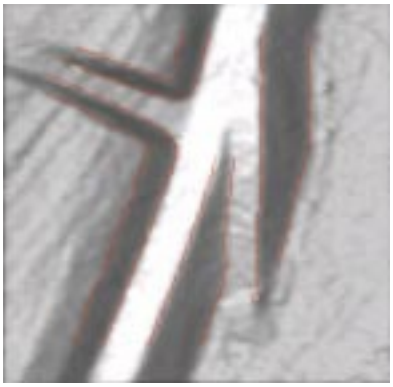

(b) Automatically extracted vector breaklines, not yet smoothed

Figure 1: Objective of approach: automatic derivation of terrain breaklines from laserdata

Up to now breaklines are measured photogrammetrically, which is a time consuming task. Deriving breaklines automatically from laserdata by means of image processing algorithms will facilitate the acquisition of this additional morphologic information. For this task, however, the density of laserpoints must be much higher than the above mentioned one point per 16 m^2.

In this contribution, some methods for the extraction of breaklines from laserdata are shortly described. The suitability of one of these methods based on hypothesis testing has been investigated. For the assessment of the performance of the algorithm, the automatically extracted breaklines are compared with photogrammetrically measured breaklines. It is shown that automatic breakline extraction from airborne laserdata in principle is feasible.

2 METHODS FOR BREAKLINE DETECTION

The output of a range image sensor, e.g. a laseraltimeter, is the scene surface geometry in sampled form. It is most commonly represented as a two-dimensional array of pixels, each pixel representing the range of a sampled point on the surface from a reference point. The role of segmentation is to extract geometric primitives relevant to higher level cognitive processes from the pixel-level representation. In the context of range image segmentation, the simplest possible geometric primitives are continuous surface patches and surface discontinuities. Likewise, most surface segmentation techniques can be classified as either edge-based or region-based.

The key idea behind region-based range image segmentation is to estimate the surface curvature at each range pixel and cluster range pixels with homogeneous surface curvature properties. Against that, the basic idea behind edge-based range image segmentation techniques is to detect significant surface discontinuities and classify them as jump, crease or curvature edge (see fig. 2 and tab.1). Jump edges can be detected using standard edge operators designed for intensity images such as the gradient, Sobel, Kirsch, Laplacian of Gaussian, and Canny edge operators (Suk and Bhandarkar, 1992). Detection of crease and curvature edges, however, requires specialized operators. Once edge pixels have been detected and classified, they are linked together to form surface discontinuity contours.

Seeking for breaklines in *filtered* laserdata, where houses, trees and bushes have been removed, we will concentrate on *edge-based* segmentation techniques and, moreover, on the detection of *curvature* edges because jump edges (e.g. in case of buildings) hardly appear in filtered data. In the following, we will shortly describe some edge-based segmentation techniques for range images.

2.1 First derivatives and borders of sloped areas

(Gomes-Pereira and Wicherson, 1999) used first derivatives for the automatic extraction of breaklines from digital surfaces. Pixels were labelled as 'slope pixel' or 'flat pixel' corresponding to their tilt in x- or y-direction. Breaklines are then detected as borders between slope and flat areas by checking the 8-neighbourhood of every flat pixel. If at least one slope pixel is present, the center pixel is classified as breakline pixel. The resulting breaklines were rather fragmented.

2.2 Laplacian and LoG

In (Gomes-Pereira and Janssen, 1999) the Laplacian operator is applied for the breakline detection task. In comparison with a manually derived reference dataset, much more breaklines have been detected by the automatic procedure. This

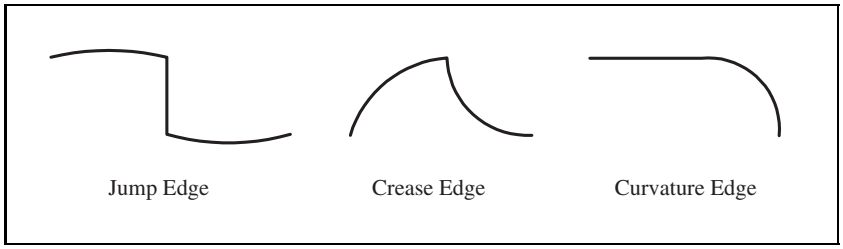

Figure 2: Different edge types

edge type	discontinuity in	continuity in
jump edge	range	
crease edge	surface normal	range
curvature edge	curvature	range and surface normal

Table 1: Characteristics of edge types

can partly be accredited to the noise strengthening effect of the second derivatives. Avoiding this effect (Chakreyavanich, 1991) uses the Laplacian of Gaussian operator (LoG) for the detection of breakpoints. The Laplacian of Gaussian operator is a combination of a Laplacian operator (∇^2) and a Gaussian function $G(c,r)$ with c = column, r = row:

$$\text{LoG} = \nabla^2 G(c,r) = \frac{c^2 + r^2 - 2s^2}{s^4} G(c,r) \quad \text{with} \quad s = \sigma_{Gaussian} \quad . \tag{1}$$

According to (Chakreyavanich, 1991), breakpoints (curvature edges) correspond to the points having positive maximum and negative minimum convoluted value of the signal between zero-crossings of LoG. Zero-crossings of the LoG represent jump edges or inflection points.

2.3 Edge preserving filtering

(Weidner, 1994) proposes an algorithm for parameterfree information-preserving surface restoration. The basic idea is to extract the data's signal and noise properties simultanously by variance-component estimation and use this information for the filtering of the data. This way discontinuities in the data are maintained. A similar idea is used by (Wild and Krzystek, 1996) in the course of an automatic DEM generation process from stereo-photographs.

2.4 Second derivatives and hypothesis testing

(Förstner, 1998) proposes to treat breakline detection in range images on principle as finding edges in intensity images by means of performing hypothesis testing. Edge pixels are meant to be borders of homogeneous regions. Therefore the following two properties are inherent to them:

1. A further to be defined homogeneity measure is significantly larger at edges than in homogeneous regions.
2. This homogeneity measure is locally maximal across the edge.

Following these principles a pixel with a significant large homogeneity with respect to noise will be called *'edge pixel'*. Thus edge pixels — actually being pixels which are non-homogeneous — indicate where there may be a signal, e.g. an edge.

For intensity images $g(c,r)$ often the squared gradient magnitude is used as homogeneity measure:

$$h_1 = |\nabla g|^2 = g_c^2 + g_r^2 \tag{2}$$

which becomes — being weighted assuming constant noise σ_n^2 — the χ_2^2-distributed test statistic

$$z_1 = \frac{h_1}{\sigma_{n'}^2} = \frac{|\nabla g|^2}{\sigma_{n'}^2} = \frac{g_c^2}{\sigma_{n'}^2} + \frac{g_r^2}{\sigma_{n'}^2} \quad . \tag{3}$$

That means that pixels with

$$z_1 > \chi_{2,\alpha}^2 \tag{4}$$

are significantly non-homogeneous, thus likely to be edge pixels. In multichannel images such as color images this test statistics can be extended to

$$z_{1_{multi}} = \sum_{k=1}^{K} \frac{h_{k;1}}{\sigma_{n_k'}^2} = \sum_{k=1}^{K} \frac{|\nabla g_k|^2}{\sigma_{n_k'}^2} \qquad \text{with} \quad K = \text{ number of channels} \ , \tag{5}$$

which now is χ^2_{2K}-distributed. This way the information of the different channels can easily be combined to a single and sensible homogeneity measure.

Transfering this principle to range images $d(c,r)$ can be realized by starting with the gradient image $\boldsymbol{g} = \nabla d = (d_c, d_r)^\top$ as two-channel image (Förstner, 1998). This is due to the fact that edges in range images are pixels which do not lie on flat surfaces but are expected to be pixels where the *curvature* — which is closely related to the *second* derivatives — is significant compared to noise. Thus instead of deriving homogeneity h_1 from the first derivatives, the homogeneity h_2 is derived from the second derivatives assuming constant noise variance:

$$\begin{aligned} h_2 &= h_1(d_c) + h_1(d_r) \;=\; (d_{cc}^2 + d_{cr}^2) + (d_{rc}^2 + d_{rr}^2) && (6)\\ &= d_{cc}^2 + 2d_{cr}^2 + d_{rr}^2 && (7)\\ &= tr\,\boldsymbol{H}^2(d) \;=\; \lambda_1^2(\boldsymbol{H}) + \lambda_2^2(\boldsymbol{H}) && (8)\\ &= \kappa_1^2 + \kappa_2^2 \quad . && (9) \end{aligned}$$

κ_1 and κ_2 are the principal curvatures which specify the curvature of surface curves in the directions of maximal and minimal normal curvature at each point. They are a perfect pair of surface curvature descriptors, which are analytically equivalent to the mean and Gaussian curvature pair (Besl, 1986). Eq.(9) only applies if the local metric is neglected. Then the 2×2 Weingarten matrix (shape operator) transforms into the Hessian matrix $\boldsymbol{H}$ (Weidner, 1994). The so-called *'quadratic variation'* h_2 is only zero in case the pixel's surrounding is flat, that is in case both principle curvatures are zero. Normalization of eq.(7) with the noise variances leads to the χ^2_3-distributed test statistics

$$z_2 = \frac{d_{cc}^2}{\sigma_{n_{cc}}^2} + \frac{d_{cr}^2}{\sigma_{n_{cr}}^2} + \frac{d_{rr}^2}{\sigma_{n_{rr}}^2} \quad . \qquad (10)$$

3 SUGGESTED APPROACH

The suggested approach is based on the latter described method of breakline detection by hypothesis testing. Fig.3 shows an overview of the performed steps. Input is an greyvalue image representing the range data. The processing chain results in smooth 3D vector breaklines. In the following we describe the single processing steps more detailed. The interim results for the small dike testdata-set (fig. 1) are illustrated in fig. 4.

3.1 Detection of possible breakpixels

Since range data often is fair noisy and, moreover, noise is strongly strengthened by every derivation, it is sensible to perform a smoothing before or during building the second derivatives which are required for calculating the homogeneity measure (see eq.(7)). To perform smoothing and derivation in one step, the differentiation kernels for determining the second derivatives could be discrete approximations of the corresponding Gaussian's (Förstner, 1998)

$$\frac{\partial^2}{\partial c^2} G_s(c,r) = \frac{c^2 - s^2}{s^4}\, G_s(c,r)\ , \qquad \frac{\partial^2}{\partial c \partial r} G_s(c,r) = \frac{cr}{s^4}\, G_s(c,r)\ , \qquad \frac{\partial^2}{\partial r^2} G_s(c,r) = \frac{r^2 - s^2}{s^4}\, G_s(c,r) \qquad (11)$$

$$\text{with} \quad G_s(c,r) = Gaussian \quad \text{and} \quad s = \sigma_{Gaussian} \quad . \qquad (12)$$

To build the test statistics z_2 in equation, the noise variances in equation (10) can explicitly be derived. For the case of the Gaussian kernels they are (Förstner, 1998):

$$\sigma_{n_{cc}}^2 = \sigma_{n_{rr}}^2 = \frac{3}{16\pi s^6}\sigma_n^2 \qquad \text{and} \qquad \sigma_{n_{cr}}^2 = \frac{1}{16\pi s^6}\sigma_n^2 \quad . \qquad (13)$$

The choice of the appropriate filter size must carefully be done because noise has to be smoothed whereas significant edges should still be detected. (Chakreyavanich, 1991) proposes to determine the correct filter size by the relationship between spatial and frequency parameters of the Gaussian. The image noise σ_n^2 can be measured in flat surface regions or estimated from homogeneous image regions (see (Förstner, 1998)). Fig. 4a shows the test statistics z_2 per pixel. The lighter the greyvalue the larger the test statistics, that is the larger the curvature in this point of the surface. Fig.4b denotes possible breakpoint regions resulting from hypothesis testing ($z_2 > \chi^2_{3,\alpha}$, with $\chi^2_{3,0.99} = 11.34$).

3.2 Nonmaxima-suppression

To reduce broad breakpoint regions to one pixel wide breaklines a simple thinning operation is not suitable because neighbouring breakpoint regions sometimes melt (see left ascent in fig. 4b). Thinning would extract the middle axis of the melted region, thus falsifying the position of the edge. In order to avoid this, a nonmaxima-suppression is performed taking into account the direction of the maximum curvature which usually is the direction across the edge. The position of the breakpixel is found as the local maximum of z_2. The direction of the maximum curvature corresponds with the direction of the eigenvector of the maximum eigenvalue of the Hessian matrix. After the nonmaxima-suppression a thinning operation is performed to eliminate cornerpixels. The pixels of the breakline then are 4-connected instead of 8-connected (fig. 4c). The heights of the pixels are taken from a slightly smoothed surface to eliminate the influence of noise.

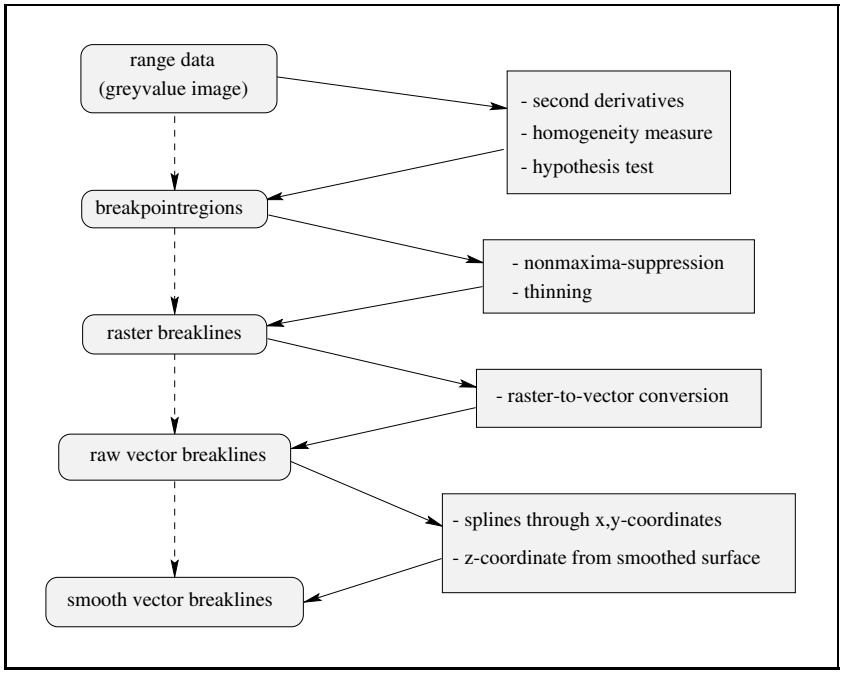

Figure 3: Flowdiagram of proposed strategy

(a) test statistics z_2

(b) breakpoint regions after hypothesis testing

(c) breakpoints after non-maxima suppression

(d) spline interpolated vector breaklines

Figure 4: Interim results of dike testdata-set

3.3 Raster-to-vector conversion

A primitive raster-to-vector conversion first transforms the pixelchain in one-pixel long 3D-vectors which point from one pixelcentre to the following pixelcentre. This yields rather zigzag breaklines. A cubic polynomial splining method is used for generalizing the lines in the x/y-coordinates. Splines with a vertice distance of three pixels yield rather smooth breaklines without a too strong generalization of the lines shapes (fig. 4d).

4 EXPERIMENTS AND RESULTS

In this section we describe the used laserdata and the obtained results of the described approach. Beside a qualitative description of the results, a quantitative assessment have been performed using photogrammetrically extracted breaklines as reference data.

4.1 Laser data

The testarea is situated along the river IJssel (The Netherlands). The flight took place in March so that the disturbing influence of leaves was minimal on the laser measurements. The dataset was acquired with the helicopter based FLI-MAP scanner. The helicopter flew at a speed of 14 m/sec and a mean height of 70 m. With a pulse frequency of 8000 Hz

and a scanning angle of $\pm 30^{\circ}$, a swath width of 61 m and a point density of approximately 7 points per square meter were achieved. More technical details are described in (Huising and Gomes-Pereira, 1998) and (Reed, 1997). From the irregularly distributed points a grid with a spacing of 0.5 m was derived by planar interpolation on a TIN.

The chosen testdataset (see fig. 5) comprises 572 $\times$ 1448 pixels, thus $286 \times 724\, m^2$. One greyvalue interval corresponds to a height difference of $5\, cm$. This part of the data mainly contains a typical Dutch dike whose dimensions are shown by the dike profile below (fig. 6). Besides we can see a farm, some trees and bushes and mostly flat meadows. Though in our experiments we use *filtered* data — where trees and houses have been eliminated — in fig. 5 the *unfiltered* data is shown in order to give a better impression of spatial proportions.

4.2 Results

From the testdataset the breaklines have automatically been derived with the approach described in section 3. The filtersize of the used Gaussian for computing the second derivatives was 25×25 pixels with $s = \sigma_{Gaussian} = 2.5$ greyvalues and $\sigma_{noise} = 5.0$ greyvalues. Fig. 5b shows the extracted vector breaklines.

4.2.1 Qualitative assessment First of all, assessing the results by visual inspection, we can state that the existing surface breaklines have rather good been detected. The four edges (two upper and two lower) of the dike are found fairly complete. However, also some small spurious breaklines have been detected. But most of the breaklines are continous long lines, nearly without interrupting gaps. Even in case of roads crossing the dike, thus forming ascents on the dike, the procedure gives reasonable results, that is the breaklines follow the direction of the curves (see fig. 5 and fig. 4d). Furthermore, a dike profile with the extracted breaklines (fig. 6) shows that the position of the extracted breaklines well complies with what a human operator would assign as points of largest curvature. Beside such a pure qualitative assessment, also some quantitative description of the results with use of reference data has been done. The following subsection deals with this matter.

4.2.2 Quantitative assessment The extracted breaklines are compared with photogrammetrically measured breaklines (see fig. 5a). These form a subset of the Dutch river database, a digital topographic dataset for rivers which is acquired by the Survey Department of Rijkswaterstaat at a generalization scale of $1:5000$. The underlying aerial color photographs are taken at a scale of $1:4000$. Before using them for the standard photogrammetric proces in a digital photogrammetric workstation, they have been scanned with a pixelsize of $12.5\, \mu m$ which corresponds with $5\, cm$ in the real world. On the one hand, the precision of these reference breaklines depends on the photogrammetric measurement precision for line elements which is supposed to be about $\sigma_{x,y(line)} = 45\, \mu m$ in the image (Kraus, 1986) and, on the other hand, on the uncertainty of the position definition of the elements to be measured. The precise locations of breaklines, of course, are less sharp defined than the position of other topographic objects such as house or road outlines. Therefore, we assume a so-called 'definition precision' of $\sigma_{x,y(def)} = 50\, cm$. This results in a x/y-precision of $\sigma_{x,y} = 53\, cm = ((4000 \cdot 0.0045)^2 + 50^2)^{1/2}\, cm$.

The river database does not cover the whole country but a certain range from the river's axis onwards (the river bed up to the dikes). For that reason the reference breaklines are missing in the upper left part of the testdataset (see fig. 5a). Another difficulty with the reference data is evident: the river database contains breaklines which are not found at all by the automatic extraction process. In the river database these breaklines are called 'soft breaklines', indicating that they rather denote contour-lines than breaklines at strong surface curvatures. Furthermore, the reference dataset is not really 3D. Every vector is supplied with only a single height-label. Therefore we restrict the quantitative assessment to the *position*, that is the x/y-co-ordinates.

For a vector based analysis, we measured distances between vectors of the two datasets, performing a sort of discrete integration of the area between the vector breaklines. Fig.7 illustrates the way this is done. Additional vertices have been inserted between the vertices of the photogrammetrically measured breaklines with a distance of $1\, m$ respectively. Then the distance from each of these points (vertices) to the nearest vector of the other set, the automatically extracted (laser-)breaklines, is computed. Thereby the search radius, that is the maximum distance for which the distance will be determined, is set to $3\, m$. From about 7000 distances a mean distance of $0.59\, m$ has been computed and the following percentages of distances have been found:

$$35\% < 0.25\, m, 60\% < 0.5\, m, 80\% < 1\, m \text{ and } 92\% < 1.5\, m.$$

As the precision of the differences resembles the order of magnitude of the precision of photogrammetric breaklines, we conclude that the automatically extracted breaklines hold a comparable x/y-precision to photogrammetric ones.

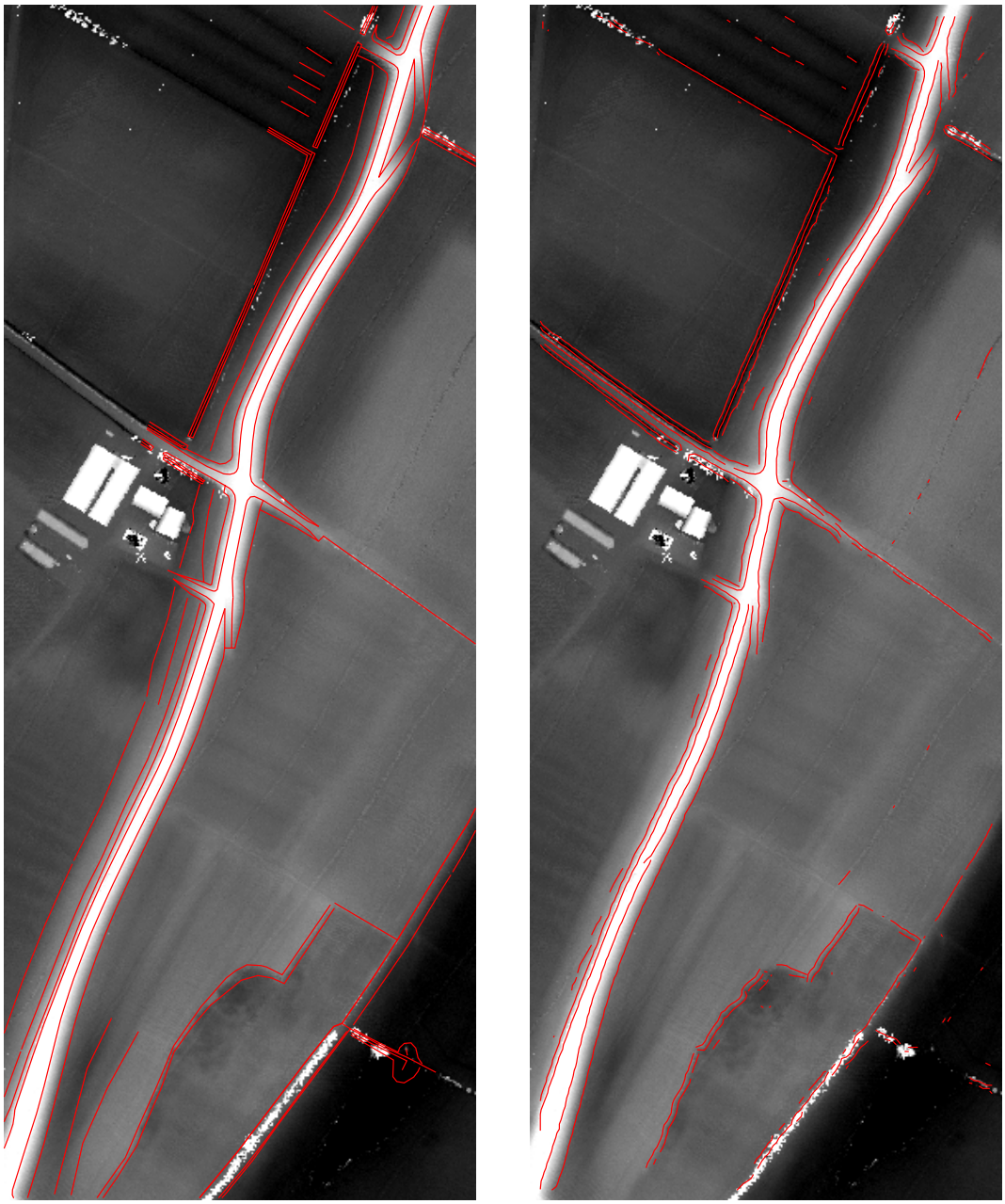

(a) Photogrammetrically measured breaklines

(b) From laserdata extracted breaklines

Figure 5: Opposition of reference breaklines against extracted breaklines

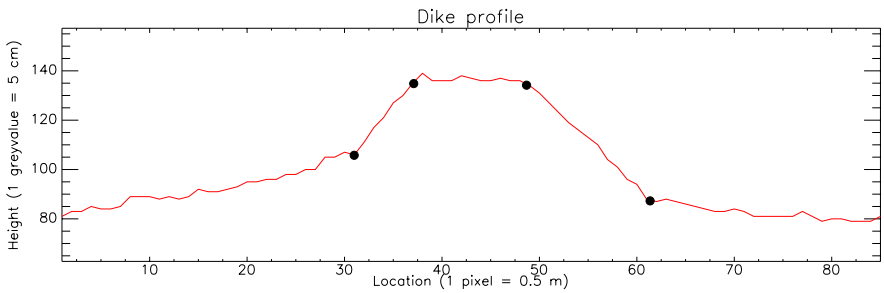

Figure 6: Dike profile with position of automatically extracted breaklines (black dots)

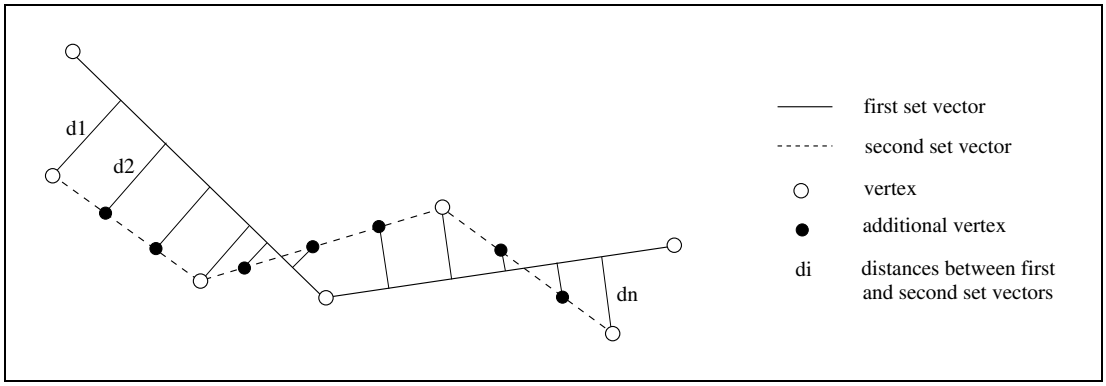

Figure 7: Distances between two sets of vectors

5 CONCLUSIONS

It is shown that automatic breakline extraction from airborne laserdata in principle is feasible. The quality of the extracted breaklines is rather good, but stays slightly behind the photogrammetrically measured breaklines. The latter technique has the advantage of simultaneously obtaining semantic information about the measured objects. Nevertheless, there are applications which do not require such explicit semantic information, e.g. data reduction or derivation of morphologic correct DEM's. Concerning the geometric aspects (apart from the semantic meaning), further investigations must show whether automatically extracted breaklines are in the same measure suited for various applications as photogrammetrically measured breaklines.

REFERENCES

Besl, P., 1986. Surfaces in Range Image Understanding. Springer.

Chakreyavanich, U., 1991. Regular Grid DEM Data Compression by Using Zero-Crossings: The Automatic Breakline Detection Method. PhD thesis, Columbus: Ohio State University. Report OSU-DGSS No. 412.

Förstner, W., 1998. Image processing for feature extraction in digital intensity, color and range images. In: Proc. Of the International Summer School on 'Data Analysis and Statistical Foundations of Geomatics', Greece, May, 25 Pp., Springer Lecture Notes on Earth Sciences.

Gomes-Pereira, L. and Janssen, L., 1999. Suitability of laser data for DTM generation: A case study in the context of road planning and design. ISPRS Journal of Photogrammetry & Remote Sensing 54, pp. 244–253.

Gomes-Pereira, L. and Wicherson, R., 1999. Suitability of laser data for deriving geographical information - a case study in the context of management of fluvial zones. ISPRS Journal of Photogrammetry & Remote Sensing 54(2-3), pp. 105–114.

Huising, E. and Gomes-Pereira, L., 1998. Errors and accuracy estimates of laser data acquired by various laser scanning systems for topographic applications. ISPRS Journal of Photogrammetry & Remote Sensing 53, pp. 245–261.

Kraus, K., 1986. Photogrammetrie. Vol. I, Dümmler Bonn.

Petzold, B., Reiss., P. and Stössel, W., 1999. Laser scanning - surveying and mapping agencies are using a new technique for the derivation of digital terrain models. ISPRS Journal of Photogrammetry & Remote Sensing 54(2-3), pp. 95–104.

Reed, M., 1997. Fugro FLI-MAP system. EARSeL Newsletter, Special Issue: Laser Scanning pp. 18–21.

Suk, M. and Bhandarkar, S., 1992. Three-Dimensional Object Recognition from Range Images. Springer.

Weidner, U., 1994. Information-preserving surface restoration and feature extraction for digital elevation models. In: Poceedings of ISPRS Commission III Symposium 'Spatial Information from Digital Photohrammetry and Computer Vision', Munich.

Wild, D. and Krzystek, P., 1996. Automatic breakline detection using an edge preserving filter. In: International Archives of Photogrammetry and Remote Sensing, Vol. XXXI, Part B3, Vienna, pp. 946–952.